Complex earthquake rupture and local tsunamis

Eric L. Geist
U.S. Geological Survey, Menlo Park, California, USA

Received 8 January 2001; revised 20 September 2001; accepted 27 September 2001; published 2 May 2002

[1] In contrast to far-field tsunami amplitudes that are fairly well predicted by the seismic moment of subduction zone earthquakes, there exists significant variation in the scaling of local tsunami amplitude with respect to seismic moment. From a global catalog of tsunami runup observations this variability is greatest for the most frequently occurring tsunamigenic subduction zone earthquakes in the magnitude range of $7 < M_w < 8.5$. Variability in local tsunami runup scaling can be ascribed to tsunami source parameters that are independent of seismic moment: variations in the water depth in the source region, the combination of higher slip and lower shear modulus at shallow depth, and rupture complexity in the form of heterogeneous slip distribution patterns. The focus of this study is on the effect that rupture complexity has on the local tsunami wave field. A wide range of slip distribution patterns are generated using a stochastic, self-affine source model that is consistent with the falloff of far-field seismic displacement spectra at high frequencies. The synthetic slip distributions generated by the stochastic source model are discretized and the vertical displacement fields from point source elastic dislocation expressions are superimposed to compute the coseismic vertical displacement field. For shallow subduction zone earthquakes it is demonstrated that self-affine irregularities of the slip distribution result in significant variations in local tsunami amplitude. The effects of rupture complexity are less pronounced for earthquakes at greater depth or along faults with steep dip angles. For a test region along the Pacific coast of central Mexico, peak nearshore tsunami amplitude is calculated for a large number ($N = 100$) of synthetic slip distribution patterns, all with identical seismic moment ($M_w = 8.1$). Analysis of the results indicates that for earthquakes of a fixed location, geometry, and seismic moment, peak nearshore tsunami amplitude can vary by a factor of 3 or more. These results indicate that there is substantially more variation in the local tsunami wave field derived from the inherent complexity subduction zone earthquakes than predicted by a simple elastic dislocation model. Probabilistic methods that take into account variability in earthquake rupture processes are likely to yield more accurate assessments of tsunami hazards. *INDEX TERMS:* 4564 Oceanography: Physical: Tsunamis and storm surges; 7215 Seismology: Earthquake parameters; 3250 Mathematical Geophysics: Fractals and multifractals; 3210 Mathematical Geophysics: Modeling; *KEYWORDS:* tsunami, slip, subduction zone, stochastic, fractal

1. Introduction

[2] Shallow subduction zone earthquakes are one of the most common sources of destructive tsunamis in the world. Events such as the 1960 Chile and 1964 Alaska earthquakes resulted in large displacements of the seafloor that were transferred as gravitational instabilities in the ocean: the tsunami. Although subduction zone events most frequently generate high local tsunami runups, it is important to note that back arc events and, to a lesser degree, outer rise events have also generated tsunamis with high runups [*Satake and Tanioka*, 1999]. To accurately assess the hazard posed by tsunamis generated by subduction zone earthquakes, it is critical that we understand how local tsunamis are affected by details of earthquake rupture.

[3] Despite differences in the underlying physics of wave propagation in the ocean and in the solid earth, the tsunami wave field emanating from an earthquake source can be thought of as an extension to the seismic wave field. *Ward* [1980] and *Okal* [1982] demonstrate that far-field tsunami waveforms can be reconstructed through the superposition of normal modes in the same way Rayleigh waves are reconstructed. Likewise, analysis of source effects on the local tsunami wave field parallels similar analyses in strong motion seismology. As detailed in this study, rupture complexity, as represented by heterogeneous slip distribution patterns, has an important effect on near-field tsunami records. The computation of the local tsunami wave field is considerably simpler than computing elastic wave propagation in the solid earth owing to the fact that the propagation velocity of long waves in the ocean is directly available from bathymetry. However, site response for tsunami waves in the form of local resonance, trapped modes of edge waves, and runup dynamics is dependent on small-scale changes in the shallow bathymetry and coastal topography and therefore is often difficult to determine accurately.

[4] In trying to reconstruct the tsunami wave field from past events, many previous studies have used a simplified elastic dislocation model constrained by the seismic moment for an earthquake. Rupture complexity is not considered in these cases, such that slip is specified as being spatially uniform over the entire rupture area or over several subevents that span the width of the rupture zone. Similarly, many tsunami hazard assessments are based on the simple dislocation model, such that the source parameters for a given seismic moment (M_0)

$$M_0 = \mu DA$$

(μ, shear modulus; D, average slip; A, rupture area) are determined from empirical scaling relationships. In general, seismic moment is

a good indicator of far-field tsunami amplitude [*Abe*, 1979; *Pelayo and Wiens*, 1992]. Near the earthquake source, however, there is substantial variation of local tsunami amplitude and runup with respect to M_0 as will be demonstrated in this paper.

[5] Previous studies [*Freund and Barnett*, 1976; *Geist and Dmowska*, 1999] have shown that nonuniform slip, particularly in the dip direction for subduction zone events, has an important effect on the static vertical displacement field and therefore tsunami generation. The alternative to the dislocation model used in tsunami studies is a crack model for the earthquake in which stress drop rather than slip is prescribed [*Geist and Dmowska*, 1999]. Slip distributions and static vertical displacement fields are calculated directly from the stress drop conditions. In particular, analytic expressions relating slip distribution to the surface displacement field [*Freund and Barnett*, 1976; *Rudnicki and Wu*, 1995] indicate that vertical displacement is affected by dip-directed gradients of slip, rather than the magnitude of slip per se. *Rudnicki and Wu* [1995] also demonstrate that an earthquake that ruptures to (or near) the surface will skew the slip distribution updip, thus enhancing the tsunamigenic potential of the earthquake [*Geist and Dmowska*, 1999].

[6] Whereas the comparison of crack and dislocation models demonstrates the fundamental effect that slip distribution has on tsunami generation, results from seismic inversions indicate that slip distributions are remarkably heterogeneous and diverse [*Beck and Ruff*, 1989; *Thatcher*, 1990]. Neither the crack nor dislocation model provides an adequate representation of the complex rupture of large subduction zone earthquakes. (The origin of rupture complexity for subduction zone earthquakes has been discussed, for example, by *Rundle and Kanamori* [1987].) In comparison to conventional dislocation models used to model tsunami generation from these earthquakes, the primary effect of slip heterogeneity is to increase the amplitude and frequency content of the local tsunami wave field, particularly for rupture areas located entirely offshore (i.e., heterogeneous slip results in concentrated patches of deformation transferred to the water column). In addition, *Geist and Dmowska* [1999] demonstrate that runup variability broadside from (i.e., directly adjacent to) the rupture zone can also be ascribed to slip heterogeneity, in combination with small-scale bathymetric changes, as in the case of the tsunami from the 1992 Nicaragua earthquake.

[7] The underestimation of amplitude and frequency characteristics by using a simple dislocation model explains a systematic discrepancy between the width of the rupture zone derived from tsunami models and the width prescribed/derived from seismic inversions. For dislocation models, decreasing the rupture width (and thus increasing slip for a given M_0) has the effect of increasing the amplitude and decreasing the wavelength of the initial tsunami [*Geist*, 1998] and therefore compensates for an oversimplification of the rupture process. This discrepancy is illustrated by the following examples: (1) for the 1992 Nicaragua earthquake a 70-km-wide rupture zone ($M_0 = 4.2 \times 10^{20}$ N m) is used in the seismic inversion of *Ihmlé* [1996], whereas a 40-km-wide rupture ($M_0 = 3 \times 10^{20}$ N m) is used in the tsunami model of *Satake* [1994]; (2) for the 1993 Hokkaido earthquake a 70-km-wide rupture ($M_0 = 3.4 \times 10^{20}$ N m) is used in the seismic inversion [*Mendoza and Fukuyama*, 1996] and a 30-km-wide rupture ($M_0 = 4.85 \times 10^{20}$ N m) is used in the tsunami model [*Satake and Tanioka*, 1995]; and (3) for the 1992 Flores Indonesia earthquake a 60-km-wide rupture ($M_0 = 7.5 - 8 \times 10^{20}$ N m) is used in the seismic inversion [*Beckers and Lay*, 1995] and a 25-km-wide rupture ($M_0 = 6.4 \times 10^{20}$ N m) for the tsunami model [*Imamura et al.*, 1995]. Although rupture width is, in general, poorly constrained in seismic inversions, the rupture width required by the uniform slip model for tsunami generation is artificially small. The tsunami wave field reconstructed using the slip distribution and width derived/prescribed from seismic inversions, on the other hand, will in most cases be consistent with local and far-field tide gauge records and runup observations.

[8] The objective of this study is to determine the effect that rupture complexity, by way of different slip distribution patterns, has on the local tsunami wave field. Because the spatial resolution of slip from seismic inversions is limited, it is important to also establish what length scale spatial heterogeneity of slip significantly affects the tsunami wave field. To do so, a stochastic source model is employed that reflects the self-similar nature of earthquake rupture. Using this source model, the range of variation in nearshore tsunami amplitudes can be gauged for earthquakes of identical seismic moment.

2. Variability of Local Tsunami Runup With Seismic Moment

[9] The variability of local tsunami runup with respect to seismic moment is first established for circum-Pacific subduction zone earthquakes from 1896 to 1996 as shown in Figure 1 and Table 1. Two tsunami scales are used for comparison: the Imamura-Iida magnitude scale m [*Iida*, 1963; *Iida et al.*, 1967] based on the maximum tsunami height

$$m = \log_2 h_{\max} \tag{1}$$

and the Soloviev-Go intensity scale i [*Soloviev*, 1970; *Soloviev and Go*, 1974] based on the mean tsunami height

$$i = \log_2 \left(h\sqrt{2} \right). \tag{2}$$

For this study, local tsunami height is determined from observations limited to within a 100-km perimeter outside of the aftershock region or rupture area. In some cases, this spatial constraint results in only a few observations attributed to a particular event. For example, although the tsunami from the M_w = 8.0 1986 Aleutian earthquake was widely recorded around the Pacific, there is only one local runup observation of 0.9 m on Adak Island [*Lander*, 1996]. Other runup observations on Unalaska (0.1 m) and the Shumagin Islands (<0.1 m) are outside the local area of the aftershocks [*Boyd and Nabelek*, 1988]. In addition, amplitude readings from tide gauge stations are occasionally not distinguished from maximum runup; where the distinction is made, tsunami runup measurements are used. Because of sparse distribution of observations and instruments along much of the Pacific coastline it is also likely that small tsunamis from subduction zone earthquakes have been underreported in the past. Despite the inherent difficulties in constructing a local tsunami catalog, it is apparent that for the most frequently occurring tsunamigenic earthquakes ($7 < M_w < 8.5$), there is considerable variability in tsunami runup as a function of seismic moment (Figure 1).

[10] Far-field scaling of tsunami amplitude with seismic moment for subduction zone earthquakes is established by *Abe* [1979, 1981]:

$$\log H = M_w - \log R - 5.55, \tag{3}$$

where H is maximum tsunami amplitude (in meters) and R is the distance from the earthquake epicenter (in kilometers). For local tsunamis, however, *Abe* [1995] indicates that the far-field relation above overestimates local tsunami heights and proposes the following local limit of tsunami height (Hr):

$$\log \mathrm{Hr} = 0.5M_w - 3.30 + C, \tag{4}$$

where $C = 0.0$ for subduction zone events and $C = 0.2$ for back arc

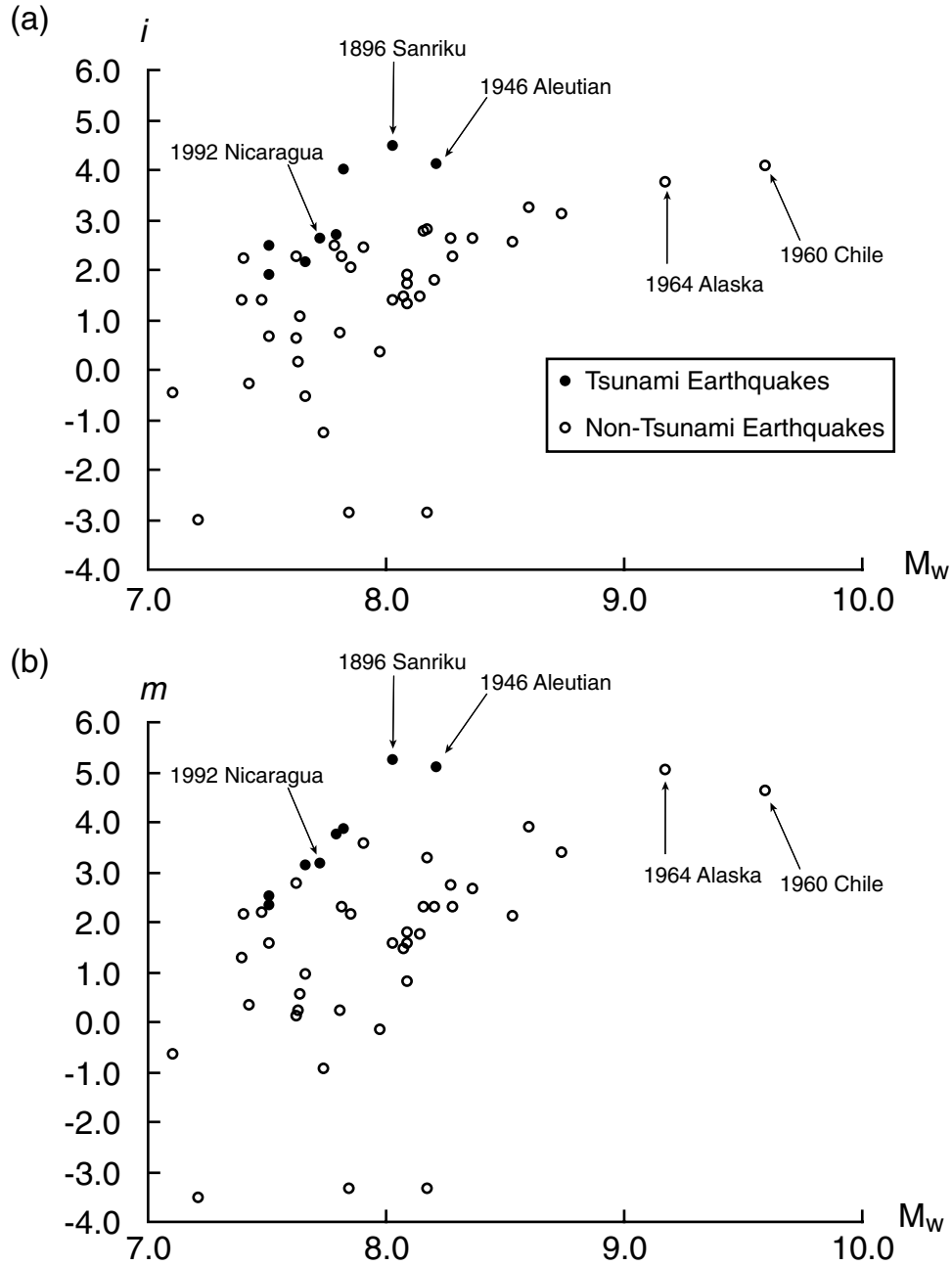

Figure 1. Moment magnitude (M_w) versus tsunami magnitude (using only local tsunami measurements) for circum-Pacific subduction zone earthquakes. Tsunami magnitude is expressed using (a) the Soloviev-Go intensity scale and (b) the Imamura-Iida magnitude scale. Solid and open circles represent tsunami and nontsunami earthquakes, respectively. Note variability of tsunami magnitude for the most frequent tsunamigenic earthquakes ($7.0 < M_w < 8.5$).

events. The high density of tsunami observations for six tsunamigenic earthquakes around Japan (excluding the 1896 Sanriku tsunami earthquake) allows *Abe* [1995] to establish meaningful statistics of local runup. *Abe* [1995] calculates a logarithmic standard deviation of 1.55 for estimated (using equation (4)) and observed local mean heights. For the circum-Pacific data set (Table 1) the logarithmic standard deviation for estimated and observed local mean heights is >3. The greater uncertainty in estimating local tsunami heights using (4) for the circum-Pacific data set is likely due to tsunami runup variations related to site-specific variations in nearshore bathymetry in combination with source variations. It should be also noted, however, that the circum-Pacific data set (Table 1) includes earthquakes of greater than magnitude 7.1, whereas the diversity of the earthquake population in Japan considered by *Abe* [1995] is limited by considering earthquakes with magnitude 7.9 or greater.

[11] The inclusion of tsunami earthquakes in examining the local runup for a particular region will substantially increase the variability of mean and maximum runup with respect to M_w (Figure 1 and Table 1). Tsunami earthquake is a term defined by *Kanamori* [1972] to refer to those earthquakes that generate a much larger tsunami than would be predicted by the surface wave magnitude (M_s) of the earthquake [see also *Pelayo and Wiens*, 1992; *Kanamori and Kikuchi*, 1993]. Slow tsunami earthquakes defined by *Polet and Kanamori* [2000, p. 684] are a subset of tsunami earthquakes that are characterized by "an anomalously

Table 1. Seismic Moment and Local Tsunami Runup From Large Subduction Zone Earthquakes in the Pacific[a]

Region	Date	M_0	M_w	Reference (M_0)	Average Local Runup	Maximum Local Runup	Reference (Runup)
				Tsunami Earthquakes			
Sanriku	15 June 1896	12.	8.0	*Tanioka and Satake* [1996]	16.0	38.2	*Abe* [1995]
Aleutians	1 April 1946	23.	8.2	*Johnson and Satake* [1997]	12.4	35.0	*Lander* [1996]
Peru	20 Nov. 1960	3.4	7.7	*Pelayo and Wiens* [1992]	3.2	9.0	*Lockridge* [1985]
Kurile	20 Oct. 1963	6.	7.8	*Pelayo and Wiens* [1992]	11.5	15.0	*Iida et al.* [1967]
Kurile	10 June 19/75	2.	7.5	*Pelayo and Wiens* [1992]	4.0	5.9	*Lockridge and Smith* [1984]
Nicaragua	2 Sept. 1992	4.2	7.7	*Ihmlé* [1996]	4.5	9.1	*Baptista et al.* [1993]
Java	2 June 1994	5.34	7.8	*Dziewonski et al.* [1995]	4.7	13.9	*Tsuji et al.* [1995]
Peru	21 Feb. 1996	2.	7.5	*Ihmlé et al.* [1998]	2.7	5.1	ITIC newsletter
				Nontsunami Earthquakes			
Kanto	1 Sept. 1923	8.	7.9	*Wald and Somerville* [1995]	3.9	12.0	*Abe* [1995]
Alaska	10 Nov. 1938	20.	8.2	*Johnson and Satake* [1994]	0.1	0.1	*Lander* [1996]
Tonankai	7 Dec. 1944	20.	8.2	*Satake* [1993]	5.0	10.0	*Abe* [1995]
Nankaido	20 Dec. 1946	39.	8.4	*Satake* [1993]	4.4	6.5	*Abe* [1995]
Aleutians	9 March 1957	88.	8.6	*Johnson and Satake* [1993]	6.7	15.0	*Lander* [1996]
Colombia	19 Jan. 1958	5.2	7.8	*Kanamori and Given* [1981]	4.0		*Lockridge and Smith* [1984]
Chile	22 May 1960	2700.	9.6	*Linde and Silver* [1989]	12.2	25.0	*Lockridge* [1985]
Kurile	13 Oct. 1963	70.	8.5	*Beck and Ruff* [1987]	4.2	4.4	*Iida et al.* [1967]
Alaska	28 March 1964	630.	9.2	*Johnson et al.* [1996]	9.5	34.5	*Lander* [1996]
Aleutians	4 Feb. 1965	53.	8.4	*Johnson and Satake* [1996]	6.2	10.7	*Lander* [1996]
New Hebrides	11 Aug. 1965	3.	7.6	*Ebel* [1980]	3.5	7.0	*Lockridge and Smith* [1984]
Peru	17 Oct. 1966	2.	7.5	*Abe* [1972]	1.2	3.0	*Lockridge* [1985]
Kyushu	1 April 1968	1.8	7.5	*Shono et al.* [1976]	1.9	4.6	*Abe* [1995]
Honshu	16 May 1968	28.	8.3	*Kanamori* [1971]	4.5	6.8	*Abe* [1995]
Honshu	12 June 1968	0.5	7.1	*Yoshioka and Abe* [1976]	0.5	0.7	ITIC Newsletter
Kurile	11 Aug. 1969	22.	8.2	*Abe* [1973]	2.5	5.0	*Lockridge and Smith* [1984]
Chile	9 July 1971	5.6	7.8	*Malgrange et al.* [1981]	1.2	1.2	*Lockridge* [1985]
Solomon Islands	14 July 1971	12.	8.0	*Lay and Kanamori* [1980]	1.9	3.0	*Lockridge and Smith* [1984]
Solomon Islands	26 July 1971	18.	8.1	*Lay and Kanamori* [1980]	2.0	3.4	*Lockridge and Smith* [1984]
Middle America	30 Jan. 1973	3.	7.6	*Chael and Stewart* [1982]	1.1	1.1	*Sanchez and Farreras* [1993]
Hokkaido	17 June 1973	6.7	7.9	*Shimazaki* [1974]	3.0	4.5	*Abe* [1995]
Solomon Islands	1 Feb. 1974	1.4	7.4	*Lay and Kanamori* [1980]	3.4	4.5	ITIC Newsletter
Peru	3 Oct. 1974	15.	8.1	*Hartzell and Langer* [1993]	1.8	1.8	*Lockridge* [1985]
Solomon Islands	20 July 1975	3.4	7.7	*Lay and Kanamori* [1980]	0.5	2.0	ITIC Newsletter
Mindanao	16 Aug. 1976	19.	8.2	*Stewart and Cohn* [1979]	4.9	5.0	ITIC Newsletter
Honshu	12 June 1978	3.1	7.6	*Seno et al.* [1980]	0.8	1.2	*Lockridge and Smith* [1984]
Middle America	29 Nov. 1978	3.2	7.6	*Stewart et al.* [1981]	1.5	1.5	*Sanchez and Farreras* [1993]
Alaska	28 Feb. 1979	6.5	7.8	*Lahr et al.* [1980]	0.1	0.1	*Lander* [1996]
Middle America	14 March 1979	1.5	7.4	*Mendoza* [1995]	0.6	1.3	*Sanchez and Farreras* [1993]
Colombia	12 Dec. 1979	29.	8.3	*Kanamori and Given* [1981]	3.5	5.0	ITIC newsletter
Middle America	25 Oct. 1981	0.71	7.2	*Mendoza* [1993]	0.1	0.1	*Sanchez and Farreras* [1993]
Chile	3 March 1985	15.	8.1	*Mendoza et al.* [1994]	2.4	3.5	*Lockridge* [1985]
Middle America	19 Sept. 1985	15.	8.1	*Mendoza and Hartzell* [1989]	2.7	3.0	*Sanchez and Farreras* [1993]
Middle America	21 Sept. 1985	1.35	7.4	*Mendoza* [1993]	1.9	2.5	*Sanchez and Farreras* [1993]
Aleutians	7 May 1986	10.	8.0	*Das and Kostrov* [1990]	0.9	0.9	*Lander* [1996]
Sanriku	28 Dec. 1994	4.5	7.7	*Tanioka et al.* [1996]	0.3	0.5	ITIC Newsletter
Chile	30 July 1995	14.2	8.1	*Ihmlé and Ruegg* [1997]	2.0	2.8	*Ramirez and Titchoca* [1997]
Middle America	9 Oct. 1995	8.3	7.9	*Mendoza and Hartzell* [1999]	3.5	5.0	ITIC Newsletter

[a] Updated from compilation of *Lay et al.* [1982].

low energy release in the 1–20 s frequency band with respect to their moment magnitude." Most, if not all, slow tsunami earthquakes occur along the shallowest part of the interplate thrust near the trench [*Satake and Tanioka*, 1999]. As noted by *Abe* [1995], the local mean limiting height calculated from M_w (4) for tsunami earthquakes is consistently smaller than the observed local mean height. It is difficult to establish a local runup-M_w relationship based on past observations for subduction zones where tsunami earthquakes have repeatedly occurred such as the Peru subduction zone (tsunami earthquakes in 1960 and 1996) (Figure 2). Though it could be argued that this difficulty is attributed to the sparse number of observations prior to the 1996 event [*Bourgeois et al.*, 1999], runup from the two tsunami earthquakes is larger than the two other larger-magnitude, typical subduction zone earthquakes.

[12] The reason for the variability in the local runup-M_w relationship is that tsunami excitation depends on other parameters independent of seismic moment, including the distribution of water depth at the source, the combination of higher slip and lower shear modulus at shallow depths [*Polet and Kanamori*, 2000; *Geist and Bilek*, 2001], and rupture complexity. In addition, it is likely that many shallow subduction zone earthquakes rupture to the surface, resulting in a twofold increase in average slip for the same stress drop as ideally predicted by crack mechanics [*Shimazaki*, 1986; *Rudnicki and Wu*, 1995]. Tsunami earthquakes in particular are characterized by deep water depths overlying the rupture area and high amounts of slip [*Geist*, 1998]. Before the tsunami arrives at the shoreline, local tsunami amplification during shoaling is directly dependent on the water depth in the source area, following *Ward*'s [2001b] notation of Green's law:

$$S_L = (h/h_s)^{1/4}, \tag{5}$$

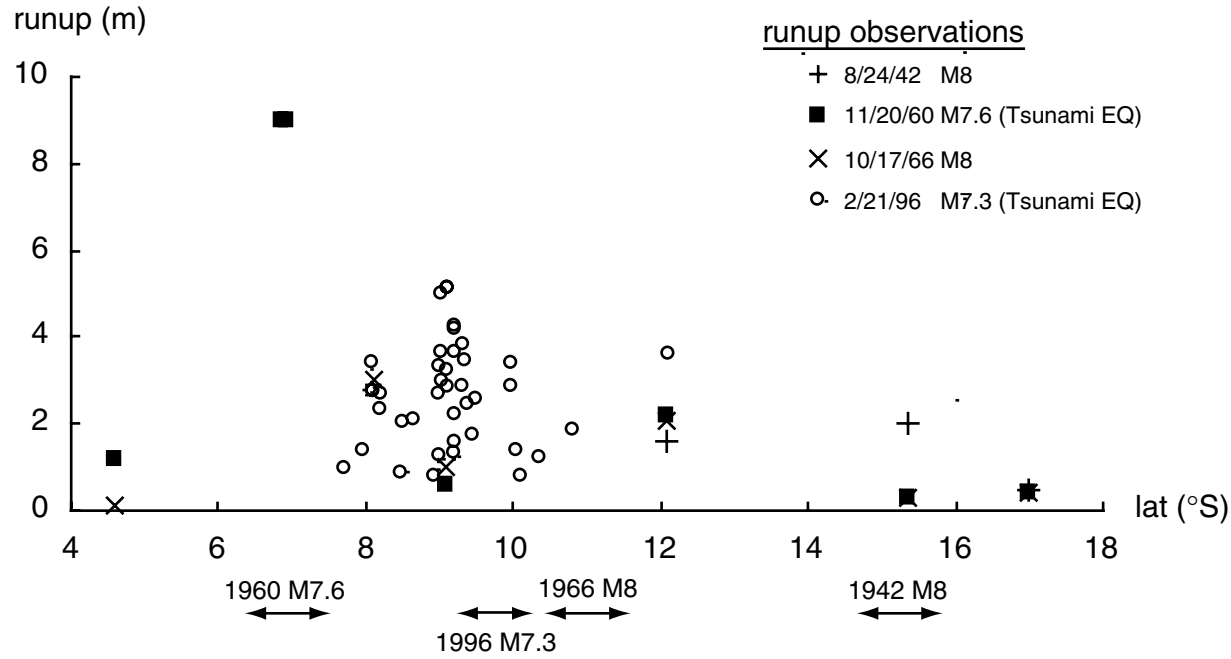

Figure 2. Runup measurements along the coast of Peru for four different earthquakes. Rupture length for each earthquake indicated by the double-headed arrows. Tsunami runup from each earthquake is largest along the stretch of coastline across from the rupture zone. The 20 November 1960 and 21 February 1996 events were tsunami earthquakes. Note that for this particular region and time period, local tsunami runup does not correlate with earthquake magnitude. The numerous runup observations from the 1996 event are from a postevent field study by *Bourgeois et al.* [1999]. Other tsunami data are from *Lockridge* [1985].

where S_L is the shoaling amplification factor and h and h_s are the water depths at the source and at a nearshore site, respectively. The fairly well defined (i.e., linear) local runup-M_w scaling relationship for tsunami earthquakes alone (Figure 1) is explained by the fact that tsunami earthquakes consistently occur at a particular position in the subduction zone such that there is little variation in tsunami source parameters described above.

3. Stochastic Source Model

[13] The difficulty in estimating the amplitude of local tsunamis from only the seismic moment of the earthquake arises from a more complex relationship between the earthquake and the initial tsunami than presumed from the uniform slip model. In particular, strong heterogeneity in coseismic slip distribution fields results not only in spatial variations in tsunami amplitude but also fundamental changes to the tsunami wave profile [*Geist and Dmowska*, 1999]. Accurate representation of the tsunami wave profile is critical toward estimating local tsunami runup. *Togashi* [1983], *Pelinovsky and Mazova* [1992], *Tadepalli and Synolakis* [1994, 1996] and others have shown that parameters such as leading wave steepness, polarity, and amplitude ratio of the leading phases all have a significant effect on tsunami runup. The most accurate representation of the local tsunami wave field is therefore derived from complete knowledge of how slip is distributed throughout the area of rupture.

[14] Slip distribution derived from seismic inversions can provide a basis for investigating the relationship between source complexity and local tsunamis. In an examination of seismic inversions from different types of earthquakes, *Mai and Beroza* [2000] indicate that fault slip varies at all resolvable length scales for dip-slip events. It is possible, however, that slip heterogeneity at scales less than what can be resolved by teleseismic data may effect the tsunami wave field. In one dimension, *Geist and Dmowska* [1999] compare the analytic coseismic vertical displacement profile calculated from a crack to a discretized approximation calculated from the superimposed displacement from uniform slip dislocations. They indicate that a distribution of discrete dislocations with lengths similar to the source depth can sufficiently reproduce the vertical displacement profile. To test this hypothesis for complex two-dimensional slip distributions and at scales smaller than the resolution afforded by seismic inversions, a static stochastic source model derived by *Andrews* [1980, 1981] and *Herrero and Bernard* [1994] is employed. Moreover, the stochastic slip model provides a tool to generated a broad range of slip distributions for an earthquake of a given seismic moment and location to better gauge the effect of rupture complexity on local tsunamis.

[15] Several authors have demonstrated that the ω^{-2} falloff in the seismic source spectrum for frequencies higher than the corner frequency and the b value for aftershocks is derived from a self-similar mode of rupture [*Hanks*, 1979; *Andrews*, 1980; *Fukao and Furumoto*, 1985; *Huang and Turcotte*, 1988; *Frankel*, 1991; *Koyama*, 1994; *Bernard et al.*, 1996]. The ω^{-2} model [*Aki*, 1967] is best explained by self-similar irregularities in either the initial stress or the static stress drop distribution [*Andrews*, 1981; *Huang and Turcotte*, 1988; *Frankel*, 1991; *Tsai*, 1997], indicating that fault strength is scale invariant or that stress drop scaling is constant. The Hurst exponent (H) spans the range of fractional Brownian motion such that $0 < H < 1$, where $H = 1/2$ represents ordinary Brownian motion [*Mandelbrot*, 1977; *Andrews*, 1981; *Peitgen et al.*, 1992; *Turcotte*, 1992; *Tsai*, 1997]. For the stress drop distribution described above, $H_{\Delta\sigma} = 0$, which is the case for a strictly self similar function: that is, variance of the stress fluctuations is independent of scale length. For the more general case in which the high-frequency falloff of the seismic displacement spectrum is expressed as $\omega^{-\gamma}$, the exponent γ is related to the Hurst exponent according to *Tsai* [1997]:

$$\gamma = H_{\Delta\sigma} + 2. \tag{6}$$

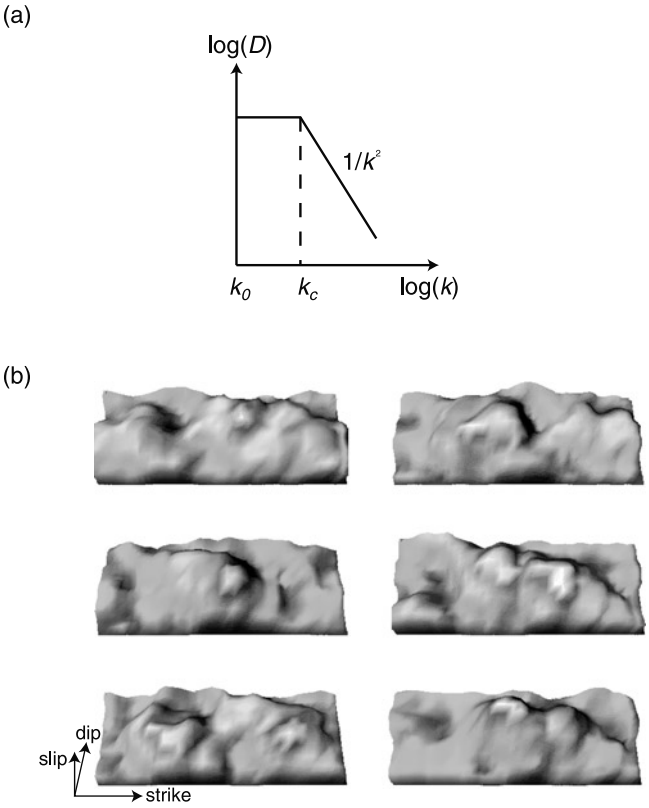

Figure 3. (a) Model radial wave number (k) spectrum for the synthetic slip distributions used in this study [*Herrero and Bernard*, 1994]. The k^{-2} falloff at high wave numbers is consistent with ω^{-2} model for the seismic source spectrum [*Aki*, 1967]. The parameter k_c is the corner wave number of the slip spectrum; k_0 is the fundamental wave number for the discrete spectrum. (b) Slip distributions produced by the stochastic model illustrating the diversity of slip distribution patterns. Light colors represent high amounts of slip. See color version of this figure at back of this issue.

Because slip and stress change for a rupture are directly related, the Hurst exponent for the slip distribution can be determined from $H_{\Delta\sigma}$ [*Tsai*, 1997]:

$$H_{\Delta\sigma} = H_u - 1. \tag{7}$$

Thus, for the case in which $H_{\Delta\sigma} = 0$, $H_u = 1$, indicating that the slip distribution borders between being self-affine (i.e., variance decreases with scale length) and differentiable [*Tsai*, 1997]. Equation (7) implies that the stress drop distribution is always rougher than the corresponding slip distribution.

[16] *Hartzell and Heaton* [1985] calculate the source spectra for a number of tsunamigenic subduction zone earthquakes. They indicate the high-frequency falloff in the displacement spectrum $\omega^{-\gamma}$ varies such that $1.0 < \gamma < 2.25$ with an average value of $\gamma = 1.5$. More recently, *Polet and Kanamori* [2000] indicate that γ for subduction zone earthquakes (not limited to low-angle thrust mechanisms) varies between 1.25 and 2.60 with an average value of $\gamma = 1.8$. The high-frequency falloff may, in fact, be more complex than can be characterized by a single exponent. For example, *Boatwright and Choy* [1992] indicate for continental earthquakes the existence of a second corner frequency such that the falloff for intermediate frequencies is approximately $\gamma = 1.5$, whereas for the highest frequencies $\gamma = 2.0$. *Koyama* [1994] suggests that the first corner frequency relates to the entire rupture process, whereas the second corner frequency reflects the average rupture characteristics of individual fault patches. The stochastic source model can be adjusted to incorporate different values of γ, according to equation (6). For the cases initially considered in the discussion below, we use a stochastic model based on $\gamma = 2$.

[17] *Andrews* [1980] and *Herrero and Bernard* [1994] demonstrate that the ω^{-2} model (i.e., $H_{\Delta\sigma} = 0$; $H_u = 1$) corresponds to a k^{-2} decay in the radial wave number spectrum of the slip distribution. Because the self-affine slip function is spatially truncated according to its seismic moment, power law scaling does not extend to wave numbers less than a corner wave number k_c (Figure 3a). (Truncation of the function may also affect the highest wave numbers of the spectrum through a leakage error described by *Bracewell* [1978].) The corner wave number varies with the characteristic rupture dimension and therefore the magnitude of the earthquake [*Somerville et al.*, 1999]. The spectrum for the lowest wave numbers is determined by low-order source parameters fixed by the seismic moment of the earthquake. The expression for the slip spectrum given by *Herrero and Bernard* [1994] is

$$\Delta u(k) = C \frac{\Delta\sigma}{\mu} \frac{L}{k^2} \qquad k > k_c, \tag{8}$$

where L is the rupture dimension and C is a constant. A stochastic model is realized by randomizing the phase for $k > k_c$. The phase for $k < k_c$ is held constant. Using this slip spectrum, slip distributions are calculated using a two-dimensional discrete Fourier transform. Discretization of the source imposes an upper limit to the power law scaling at the Nyquist wave number. The spatial discretization interval is chosen to ensure the slip spectrum at wave numbers higher than the Nyquist wave number does not have an effect on tsunami generation as discussed below. Using this model, a wide diversity of slip distribution patterns can be produced as shown in Figure 3b.

4. Modeling Nearshore Tsunami Amplitude

[18] To determine the effect that earthquake complexity has on the local tsunami wave field, numerical methods must be implemented. The coseismic vertical displacement field is calculated from the stochastic slip distribution using the point source form of elastic dislocation expressions given by *Okada* [1985] for individual small fault elements (Figure 4). The total displacement field is given by the sum of displacements from individual fault elements [*Satake and Kanamori*, 1991]. Because the objective is to establish the minimum resolution with which to accurately calculate the initial tsunami wave field, a small grid size is used in calculating both the slip distribution ($\Delta s = 2.5$ km) and seafloor displacement ($\Delta x = 1.8$ km).

[19] In discretizing the slip distribution the maximum fault element size necessary to accurately calculate seafloor deformation depends on the highest gradients of the slip distribution and the depth to the fault element. For a shallow subduction zone earthquake (3–25 km depth) on a fault dipping 14°, tests indicate that increasing Δs from 2.5 to 10 km (the spatial discretization level nominally used in seismic inversions of these earthquakes) does not significantly effect the local tsunami amplitude (variation in nearshore tsunami amplitude <10%). Therefore fault surface element dimensions (Δs) less than or equal to the source depth (d_i), can adequately represent the seafloor displacement field. Fault surface elements that are too large will incorrectly approximate the seafloor displacement field [*Geist and Dmowska*, 1999].

[20] The static elastic Green's functions for calculating seafloor displacement and the tsunami Green's functions for calculating wave elevation at the ocean surface [*Kajiura*, 1963] result in smoother irregularities of the tsunami wave field in comparison

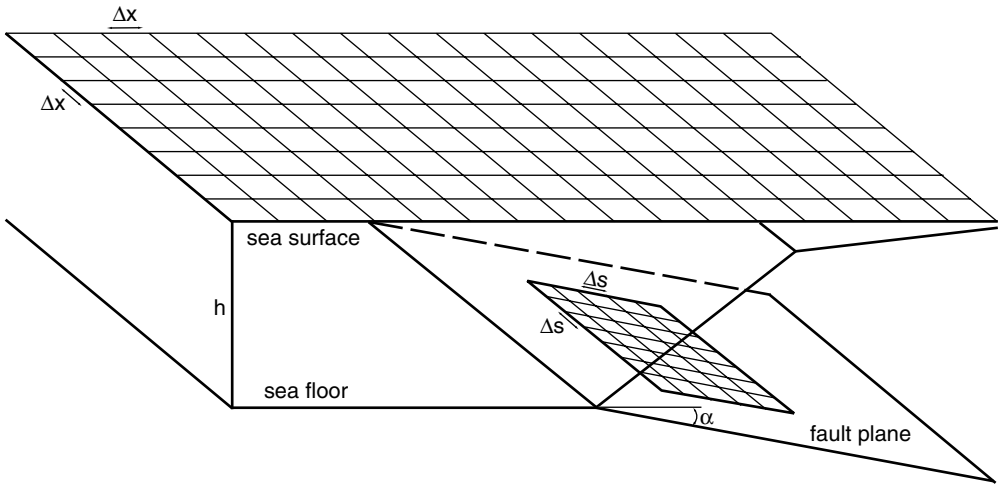

Figure 4. Schematic diagram of earthquake source and tsunami model. Coseismic vertical displacement of the seafloor is calculated from variable slip within a rupture area discretized at Δs. Coseismic displacement determines initial conditions for tsunami propagation simulated using a finite difference approximation to the linear long-wave equations with grid size Δx.

to the irregularities of slip along the fault plane. The scaling of spatial irregularities in the tsunami wave field caused by rupture complexity depends on fault dip, source depth, and, to a lesser extent, the water depth above the source region. Shallow thrust faults with a low dip angle will preserve slip irregularities in the tsunami wave field to a greater extent that earthquakes at a greater depth or along steeply dipping faults. The spectra of nearby tide gauge records include both the source effects as described above and propagation effects that have a regionally distinct spectra [*Rabinovich*, 1997].

[21] Tsunami wave propagation is calculated using the linear long wave approximation to the shallow water wave equations. The equations are numerically approximated using a leapfrog, finite difference scheme [*Aida*, 1969; *Satake*, 1993]. A nested finite difference grid is often used in tsunami modeling such that the maximum grid size (Δx, Figure 4) depends on the shortest wavelength of the tsunami [*Shuto*, 1991]. For most subduction zone earthquakes, using several grid points per wavelength results in a grid spacing of several kilometers. For tsunami models that use constant slip the initial tsunami wavelength is large (in comparison to the initial tsunami calculated from a heterogeneous slip distribution) so that a large grid spacing is used in the source region and a finer grid spacing is used in shallow water where tsunami wavelength decreases. However, for tsunami models that use heterogeneous slip it is important to realize that a fine grid spacing may be needed in the source region where most tsunami models in the past have used a large grid spacing. The time step in the finite difference scheme is governed by the Courant-Friedrichs-Lewy (CFL) stability criterion:

$$\Delta t \leq \frac{\Delta x}{\sqrt{2gh}}. \tag{9}$$

Propagation calculations are restricted to water depths greater than approximately $h = 50$ m where the nonlinear convection terms of the shallow water wave equations can be neglected [*Shuto*, 1991; *Satake*, 1995]. Reflection boundary conditions are used at this isobath. For the open ocean boundaries of the model, radiant boundary conditions are used [*Reid and Bodine*, 1968]. The linear long wave models used in this study are adequate to compute the nearshore tsunami amplitude and computationally efficient to calculate tsunamis derived from a large number of synthetic events using the stochastic source model. Tsunami runup can be estimated by applying an empirical amplification factor ($\sim$2–3 [*Shuto*, 1991; *Satake*, 1995]) to nearshore tsunami amplitude values. To explicitly compute wave propagation in water shallower than $\sim$50 m, one must include nonlinear terms, as well as a smaller grid size (thus requiring detailed coastal bathymetry and topography) to satisfy the more restrictive CFL condition and, for the runup problem, moving boundary conditions [*Shuto*, 1991; *Titov and Synolakis*, 1997]. Nearshore wave propagation has also been effectively approached using finite element methods derived from shallow water circulation models [*Myers and Baptista*, 1995]. It should be noted, also, that smaller initial wavelengths will be affected by dispersion during propagation [*Carrier*, 1971; *Shuto*, 1991]. Linear long-wave theory is adequate to model tsunami propagation for the cases considered here according to the criterion indicated by *Kajiura* [1963] and *Shuto* [1991]

$$(6h/R)^{1/3}(a/h) > 4, \tag{10}$$

where R is the propagation distance and a is the dominant width of the tsunami source. For smaller fault widths or tsunami subevent widths, dispersion effects should be considered such as under Boussinesq theory [*Carrier*, 1971; *Shuto*, 1991].

[22] Broadside from the rupture area, the largest tsunami amplitudes in many cases are traced to the direct arrival of the tsunami [cf. *Carrier*, 1995]. Along stretches of shoreline oblique to the rupture area, however, the largest tsunami amplitudes are attributed to the excitation and propagation of edge waves [*Fuller and Mysak*, 1977; *Carrier*, 1995; *González et al.*, 1995; *Fujima et al.*, 2000]. Edge waves are trapped long waves with an exponential amplitude decay in the offshore direction and are analogous to Love waves in seismology [*Sezawa and Kanai*, 1939]. Typically, only the lowest modes are excited by tsunamis [*González et al.*, 1995; *Fujima et al.*, 2000]. Phase and group velocities of edge waves depend on the shelf slope angle as discussed by *Ishii and Abe* [1980]. For irregular coastlines, edge waves will be scattered and reflected (i.e., leaky modes); where these different phases (trapped and nontrapped) constructively interfere and at antipodes, large nearshore tsunami amplitudes can be realized. Because the phase velocity of edge waves is significantly slower than nontrapped modes, these large amplitudes often occur much later than the time of the first arrival. The

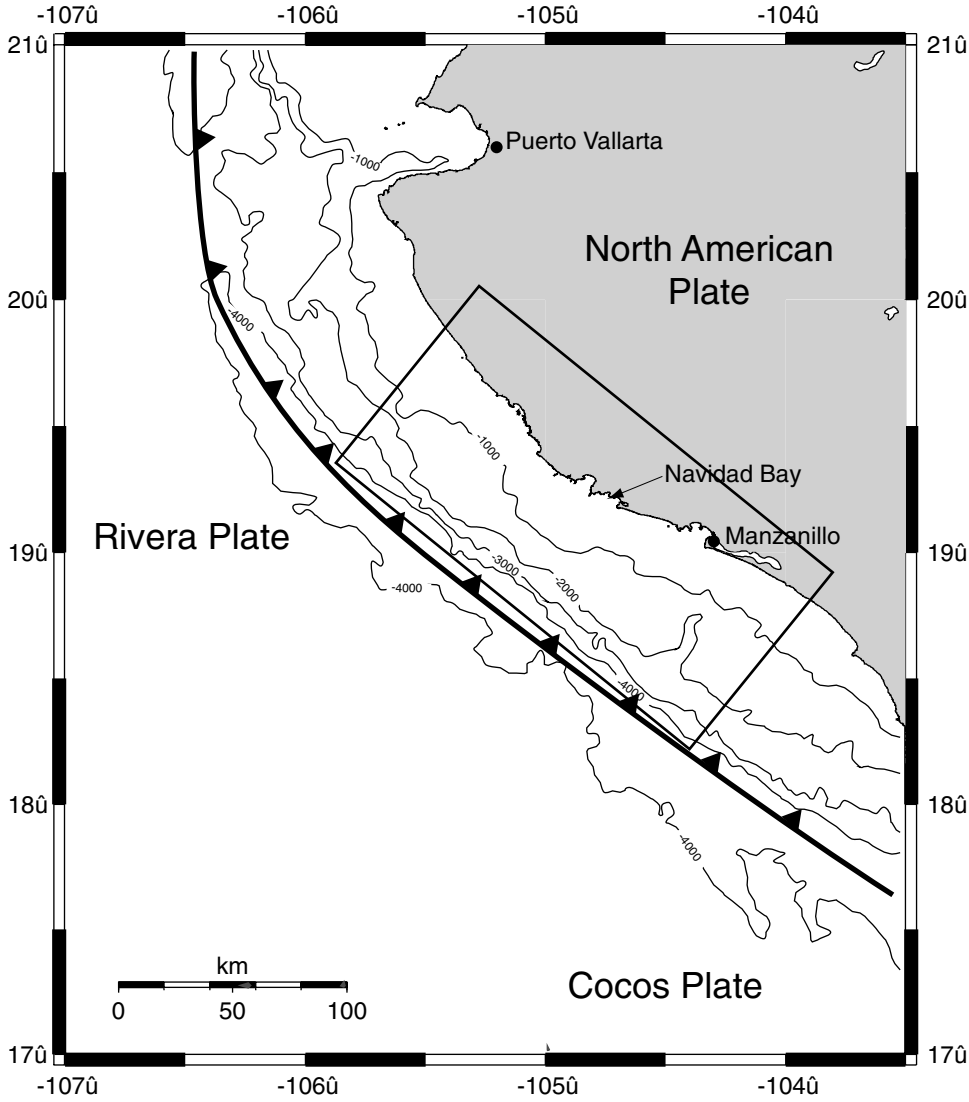

Figure 5. Location map for the region of the 9 October 1995 Colima-Jalisco M_w = 7.9 subduction zone earthquake. Surface trace of the interplate thrust shown by the heavy line. Rectangle is the rupture area used for the inversion of *Mendoza and Hartzell* [1999]. This rupture geometry is used also for the synthetics discussed in this study. Bathymetric contour interval is 1000 m.

influence of edge waves can be approximately simulated with the methods used in this study by using sufficiently long elapse times. Accurate calculation of edge wave propagation, however, involves a trade-off between using numerical methods based on irregular shoreline geometries and analytic methods that avoid numerical approximations in the nearshore region [see *Fujima et al.*, 2000].

[23] The coseismic displacement and tsunami propagation models are tested by comparing calculated tsunami waveforms with observed records. *Geist and Bilek* [2001] used a slip distribution of the M_w = 7.7 1992 Nicaragua earthquake derived from the inversion of long-period surface waves [*Ihmlé*, 1996] and a regional shear modulus function [*Bilek and Lay*, 1999] to calculate seafloor displacement and initial conditions for tsunami propagation. The computed tsunami corresponds well with observed tide gauge record. For moment distributions derived from the inversion of short-period body waves in particular, it is important that a consistent shear modulus function be used for both the seismic inversion and the conversion of moment to slip [*Geist and Bilek*, 2001]. Reductions in shear modulus in comparison to standard Earth models are supported by analysis of source durations of subduction zone earthquakes by *Bilek and Lay* [1998, 1999].

5. Effect of Rupture Complexity

[24] By holding source geometry and average slip constant (hence constant seismic moment), the stochastic source model can be used to examine the effect that different slip distribution patterns have on local tsunamis in the Colima-Jalisco region of central Mexico (Figure 5). This region was chosen primarily because large earthquakes along this subduction zone are unusually shallow [*Pacheco et al.*, 1993; *Tichelaar and Ruff*, 1993; *Suárez and Sánchez*, 1996] so that the effects of heterogeneous slip are more apparent in the tsunami wave field in comparison to other subduction zones. This region is of particular interest also because a number of earthquakes (a sequence of three in 1932 and one in 1995) have generated observed tsunamis. Reconstruction of the tsunami from the 1995 Colima-Jalisco earthquake was performed using the seismic inversion of *Mendoza and Hartzell* [1999], with good agreement to an offshore record of this event [*Filonov*, 1999].

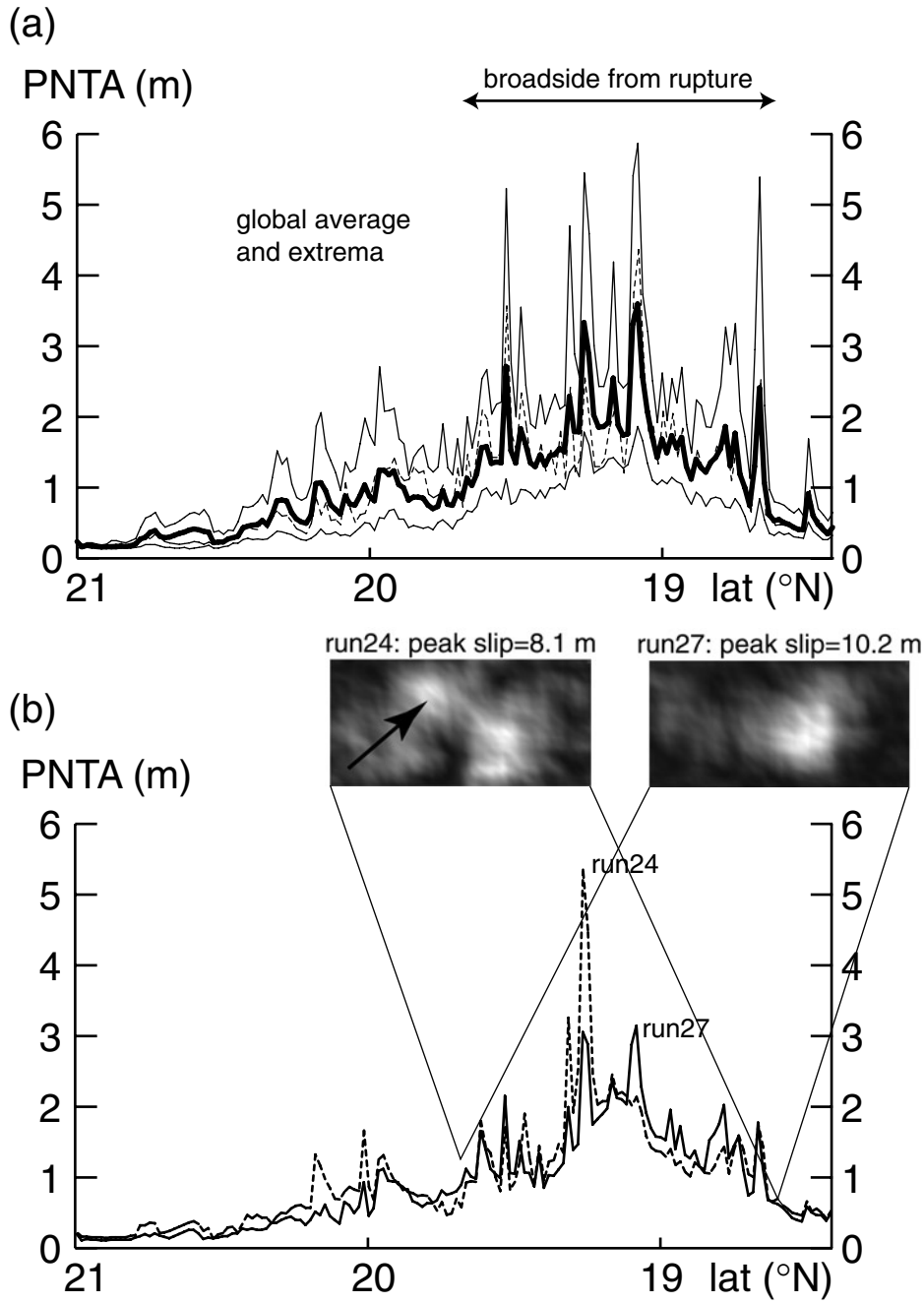

Figure 6. (a) Average and extrema peak nearshore tsunami amplitude (PNTA) calculated for 100 different slip distributions for the region shown in Figure 4. Each earthquake has identical seismic moment and location. For comparison, the PNTA for a simple elastic dislocation model (uniform slip) is shown by the dashed line. (b) PNTA for two of the slip distributions (runs 24 and 27). Lighter regions represent higher slip (average slip and seismic moment remains constant). Patch of shallow slip in run 24 results in nearshore tsunami amplitudes >5 m.

Detailed modeling of this tsunami using seismic and geodetic inversions of the earthquake is discussed by *Ortiz et al.* [2000].

[25] The predicted variability in tsunami amplitude in this region is computed using a rupture geometry identical to that of the 1995 earthquake [*Mendoza and Hartzell*, 1999]. One hundred different slip distributions are calculated using the stochastic source model. The total seismic moment for these events is $M_0 = 1.8 \times 10^{21}$ N m ($M_w = 8.1$), using a regional depth-dependent shear modulus function from *Bilek and Lay* [1999]. Calculation of seafloor displacements using *Okada*'s [1985] expressions assume a homogeneous elastic structure (in this case, a Poisson solid). The effect of elastic inhomogeneity on surface displacements and tsunami waveforms [e.g., *Yoshioka et al.*, 1989; *Geist*, 1998; *Savage*, 1998] is not included in this study. The coefficient of variation for individual slip distributions ranges between 0.59 and 0.87. The peak nearshore tsunami amplitude (PNTA) for each event is recorded at an isobath of 50 m. Extrema and average PNTA profiles for the 100 different slip distributions are plotted for each grid point parallel to the shoreline (Figure 6a). For comparison, the PNTA for a uniform slip source model is shown by the dashed line in Figure 6a. Maximum and minimum PNTA differ by a factor of ~3 on average; the largest variation in PNTA at any one

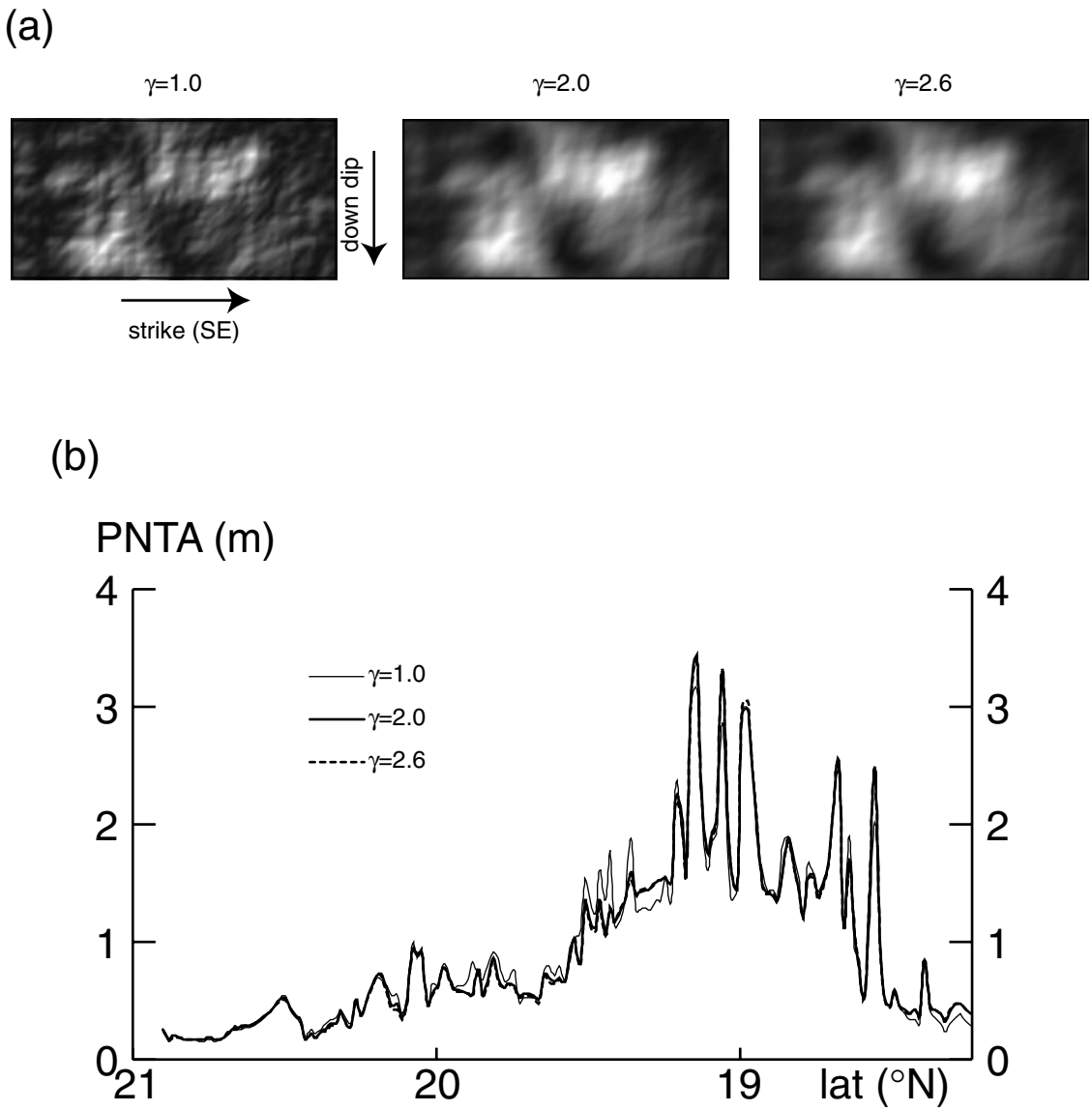

Figure 7. Effect of falloff exponent for the high wave number component of the slip spectrum (Figure 3) on peak nearshore tsunami amplitude. (a) Three slip distributions that correspond to (middle) the $\omega^{-\gamma=2}$ model, (left) lower (γ = 1.0), and (right) upper (γ = 2.6) bounds for the falloff in the seismic displacement spectra determined for subduction zone earthquakes by *Hartzell and Heaton* [1985] and *Polet and Kanamori* [2000]. Lighter regions represent higher slip (average slip and seismic moment remains constant). (b) Corresponding peak nearshore tsunami amplitude (PNTA) for each of the slip distributions in Figure 7a. Note that a rougher slip distribution (γ = 1.0) has a measurable effect on tsunami amplitude.

location along the coastline is 0.82–5.39 m (a factor of 6.6 difference). The variation in PNTA is caused by nearshore bathymetric variations and by propagation path effects from high-slip regions within the rupture zone. The latter effect is illustrated in Figure 6b. A patch of shallow slip on run 24 is responsible for the >5 m PNTA at 19.27°N. In comparison, slip distributed in the center of the rupture area (i.e., crack-like rupture) as in run 27 (Figure 6b) produces a 3-m PNTA at the same location and, overall, a PNTA profile similar to the average PNTA for the suite of 100 runs.

[26] The slope of the slip spectrum at high wave numbers has a slight effect on PNTA. As indicated previously and by *Frankel* [1991], *Bernard et al.* [1996], and *Tsai* [1997], the high-frequency falloff of the seismic displacement spectrum ($\omega^{-\gamma}$) can be linked to the slope of the high wave number falloff in the slip spectrum. Furthermore, *Polet and Kanamori* [2000] indicate that there is no general difference in the spectral falloff between tsunami earthquakes and typical subduction zone earthquakes and that in a given region, γ tends to be constant. In linking γ to changes in the Hurst exponent for slip (H_u), it is important to realize that if $H_u < 1$, then $H_{\Delta\sigma} < 0$, which is untenable under fractional Brownian motion [*Tsai*, 1997] and results in an ultraviolet catastrophic spectrum for which variance increases at shorter length scales [*Mandelbrot*, 1977; *Andrews*, 1981]. *Tsai* [1997] suggests that values of γ that result in $H_{\Delta\sigma} < 0$ may be resolved using multifractals. For slip distributions corresponding to end-member values of γ as indicated by *Hartzell and Heaton* [1985] and *Polet and Kanamori* [2000] for subduction zone earthquakes, the PNTA profiles show slight variations (Figure 7). Rougher slip distributions corresponding to $\gamma < 2$ result in greater variation in PNTA along the coastline. The

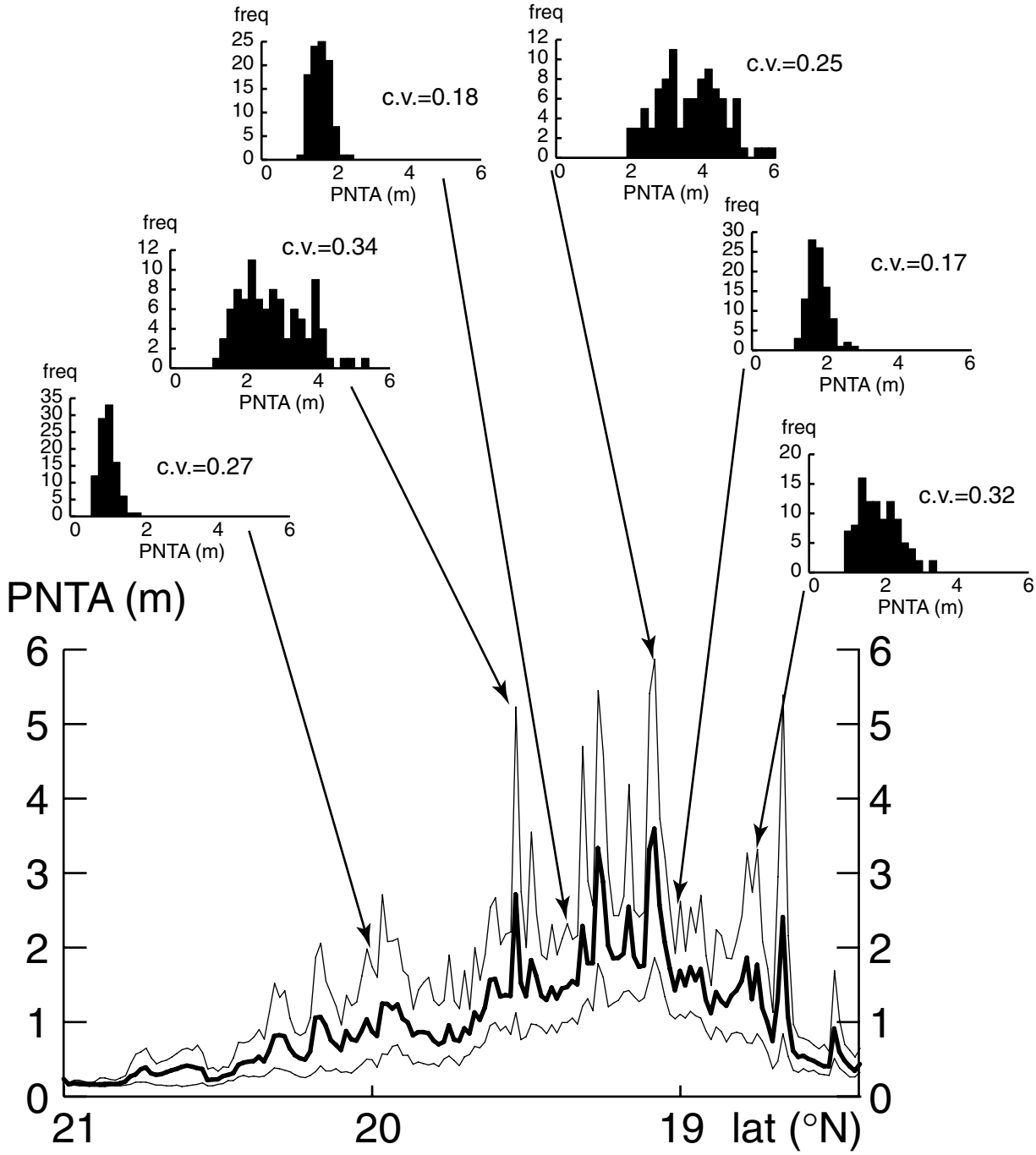

Figure 8. Histograms of peak nearshore tsunami amplitude (PNTA) at selected coastline locations for the test central Mexico rupture shown in Figure 5. Average and extrema peak nearshore tsunami amplitude are same as in Figure 6. Note complex PNTA distributions at points where tsunami amplitude is highest (c.v. is coefficient of variation).

foregoing analysis confirms that the local tsunami wave field is primarily controlled by the low wave number part of the slip spectrum, whereas the excitation of seismic waves are primarily controlled by the high wave number part of the spectrum.

6. Discussion: Implications for Local Tsunami Hazard Assessments

[27] Results from this study indicate that predictions of both local tsunami runup and seismic ground motion can be based on the same stochastic source model for earthquake rupture. Recently, various forms of the stochastic source model have also been applied to estimate strong ground motion [*Bernard et al.*, 1996; *Berge et al.*, 1998; *Hartzell et al.*, 1999; *Somerville et al.*, 1999]. Whereas computation of tsunami amplitude for a given source is relatively straightforward if bathymetry of high enough resolution is available, the computation of seismic ground motions involve strategic choices for computing the seismic Green's functions (e.g., stochastic, empirical, and theoretical [*Hartzell et al.*, 1999]). *Hartzell et al.* [1999] note for the case of the 1994 Northridge earthquake that the stochastic k^{-2} slip distribution predicts the

average characteristics of ground motion as well as the slip distribution derived from a seismic inversion of the event [*Hartzell et al.*, 1996]. The suitability of the stochastic source model is also confirmed by *Somerville et al.* [1999], who examined seismic inversions for a number of earthquakes. While the stochastic source provides a unified model with which to predict seismic ground motions as well as tsunami amplitudes, it is important to note that different components of the source wave number spectrum control generation for each wave type. Seismic waves emanating from discrete fault patches or quanta [e.g., *Rundle and Kanamori*, 1987; *Koyama*, 1994; *Rydelek and Sacks*, 1996] are primarily controlled by the high wave number, k^{-2} decay part of the spectrum, whereas as shown in this study, the local tsunami waves emanating from coseismic vertical displacement transferred to the water column are primarily controlled by the low wave number part of the spectrum near the corner wave number k_c.

[28] In contrast to tsunami hazard assessments based on a simplified elastic-dislocation representation of earthquake rupture, a large number and diversity of slip distribution patterns can be considered using the stochastic source model. For a given earthquake geometry and magnitude, results from the stochastic model are given as tsunami amplitude distributions at each point along the coastline (Figure 8). The selected histograms shown in Figure 8 indicate that at points along the coastline where tsunami amplitude is highest, the distribution of PNTA is complex and a "characteristic" PNTA associated for a given earthquake magnitude and location cannot be determined. The wide range and multipeak PNTA distribution most often occurs at promontories along the coastline and are caused by complex propagation path effects between these points and regions of high slip. At other points along the coastline where the range of PNTA is smaller, the PNTA distribution is characterized by a single peak.

[29] Results from the stochastic source model can be used as input to probabilistic hazard assessment for local tsunamis. *Ward* [2001b], *Ward and Asphaug* [2000], and *Ward* [2001a] have applied probabilistic methods, common in assessing seismic hazards, to determine the hazard for tsunamis in general and tsunamis generated by asteroid impacts and landslides in particular. *Ward* [2001b] defines the Poissonian probability that tsunami amplitude will exceed a critical value (η_{crit}) during a time interval (T) at a particular site along the coastline ($\mathbf{r}_s$) as

$$P(\mathbf{r}_s, T, \eta_{\text{crit}}) = 1 - \exp[-N(\mathbf{r}_s, \eta_{\text{crit}})T],$$

where $N^{-1}(\mathbf{r}_s, \eta_{\text{crit}})$ is the total mean recurrence interval of exceedance for all local, unobstructed tsunamigenic sources. Calculation of N requires assumptions about both the recurrence interval of tsunamigenic earthquakes and the tsunamis that are generated (as well as some understanding of the statistical uncertainty in the calculations of tsunami generation and propagation [*Ward*, 2001a]. The recurrence interval of a particular source is, most likely, the greatest unknown. Of note, statistical techniques described by *Ellsworth et al.* [1999] that take into account the aperiodicity of earthquake recurrence are likely to improve probabilistic estimates for subduction zone events. The stochastic source model can be used to generate a synthetic earthquake catalog for input into a Monte Carlo-type method for estimating tsunami hazards, similar to the technique described by *Ebel and Kafka* [1999] for estimating seismic hazards. For this method a large number of earthquake locations and magnitudes are considered in calculating ground motion probabilities. The Monte Carlo method can be adapted for tsunami hazard analysis by constructing a synthetic catalog of slip distributions for earthquakes of various magnitudes and locations and calculating the corresponding PNTA or runup.

7. Conclusions

[30] Results from this study indicate that rupture complexity of shallow subduction zone earthquakes has an important effect on the local tsunami wave field. The observed variability in local tsunami runup with respect to seismic moment is caused by rupture complexity in combination with other tsunami source parameters that are independent of seismic moment: distribution of water depth in the source region and reductions in shear modulus near the seafloor. A broad range of synthetic slip distribution patterns can be generated by the stochastic source model to gauge the variability of local tsunami amplitudes in a particular region. The high wave number component of the slip spectrum is constrained by seismic observations including the far-field falloff in the seismic displacement spectrum. A test case is considered using the rupure dimensions and location for the 1995 Colima-Jalisco earthquake and a fixed seismic moment (M_w = 8.0). For 100 different slip distributions, PNTA is shown to vary by a factor between 3 (average) and 6 (maximum) for the nearby central Mexico coastline. These results stress the importance of constructing local tsunami hazard assessments using probabilistic techniques [e.g., *Ebel and Kafka*, 1999; *Ward*, 2001b] rather than from a simplified elastic-dislocation representation of the earthquake source.

[31] **Acknowledgments.** Discussions with Joe Andrews on the stochastic source model and Modesto Ortiz on tsunamis in central Mexico greatly contributed to this study. The author thanks Pierre Ihmlé and Carlos Mendoza for seismic inversion results. The author also gratefully acknowledges constructive reviews of the manuscript by Joe Andrews, Marlene Noble, and two anonymous reviewers.

References

Abe, K., Mechanisms and tectonic implications of the 1966 and 1970 Peru earthquakes, *Phys. Earth Planet. Inter.*, *5*, 367–379, 1972.

Abe, K., Tsunami and mechanism of great earthquakes, *Phys. Earth Planet. Inter.*, *7*, 143–153, 1973.

Abe, K., Size of great earthquakes of 1837–1974 inferred from tsunami data, *J. Geophys. Res.*, *84*, 1561–1568, 1979.

Abe, K., Physical size of tsunamigenic earthquakes of the northwestern Pacific, *Phys. Earth Planet. Inter.*, *27*, 194–205, 1981.

Abe, K., Estimate of tsunami run-up heights from earthquake magnitudes, in *Tsunami: Progress in Prediction, Disaster Prevention and Warning*, *Adv. Nat. Technol. Hazards Res.*, vol. 4, edited by Y. Tsuchiya and N. Shuto, pp. 21–35, Kluwer Acad., Norwell, Mass., 1995.

Aida, I., Numerical experiments for the tsunami propagation—The 1964 Niigata tsunami and the 1968 Tokachi-Oki tsunami, *Bull. Earthquake Res. Inst. Univ. Tokyo*, *47*, 673–700, 1969.

Aki, K., Scaling law of seismic spectrum, *J. Geophys. Res.*, *72*, 1212–1231, 1967.

Andrews, D. J., A stochastic fault model, 1, Static case, *J. Geophys. Res.*, *85*, 3867–3877, 1980.

Andrews, D. J., A stochastic fault model, 2, Time-dependent case, *J. Geophys. Res.*, *86*, 10,821–10,834, 1981.

Baptista, A. M., G. R. Priest, and T. S. Murty, Field survey of the 1992 Nicaragua tsunami, *Mar. Geod.*, *16*, 169–203, 1993.

Beck, S. L., and L. J. Ruff, Rupture process of the 1963 Kurile Islands earthquake sequence: Asperity interaction and multiple event rupture, *J. Geophys. Res.*, *92*, 14,123–14,138, 1987.

Beck, S. L., and L. J. Ruff, Great earthquakes and subduction along the Peru trench, *Phys. Earth Planet. Inter.*, *57*, 199–224, 1989.

Beckers, J., and T. Lay, Very broadband seismic analysis of the 1992 Flores, Indonesia, earthquake (M_w = 7.9), *J. Geophys. Res.*, *100*, 18,179–18,193, 1995.

Berge, C., J. C. Gariel, and P. Bernard, A very broad-band stochastic source model used for near source strong motion prediction, *Geophys. Res. Lett.*, *25*, 1063–1066, 1998.

Bernard, P., A. Herrero, and C. Berge, Modeling directivity of heterogeneous earthquake ruptures, *Bull. Seismol. Soc. Am.*, *86*, 1149–1160, 1996.

Bilek, S. L., and T. Lay, Variation of interplate fault zone properties with depth in the Japan subduction zone, *Science*, *281*, 1175–1178, 1998.

Bilek, S. L., and T. Lay, Rigidity variations with depth along interplate megathrust faults in subduction zones, *Nature*, *400*, 443–446, 1999.

Boatwright, J., and G. L. Choy, Acceleration source spectra anticipated for

large earthquakes in northeastern North America, *Bull. Seismol. Soc. Am.*, *82*, 660–682, 1992.

Bourgeois, J., C. Petroff, H. Yeh, V. Titov, C. E. Synolakis, B. Benson, J. Kuroiwa, J. Lander, and E. Norabuena, Geologic setting, field survey and modeling of the Chimbote northern Peru, tsunami of 21 February 1996, *Pure Appl. Geophys.*, *154*, 513–540, 1999.

Boyd, T. M., and J. L. Nabelek, Rupture process of the Andreanof Islands earthquake of May 7, 1986, *Bull. Seismol. Soc. Am.*, *78*, 1653–1673, 1988.

Bracewell, R. N., *The Fourier Transform and its Applications*, 444 pp., McGraw-Hill, New York, 1978.

Carrier, G. F., The dynamics of tsunamis, in *Mathematical Problems in the Geophysical sciences,* no. 1, *Geophysical Fluid Dynamics*, edited by W. H. Reid, pp. 157–187, Am. Math. Soc., Providence, R. I., 1971.

Carrier, G. F., On-shelf tsunami generation and coastal propagation, in *Tsunami: Progress in Prediction, Disaster Prevention and Warning*, edited by Y. Tsuchiya and N. Shuto, pp. 1–20, Kluwer Acad., Norwell, Mass., 1995.

Chael, E. P., and G. S. Stewart, Recent large earthquakes along the Middle American trench and their implications for the subduction process, *J. Geophys. Res.*, *87*, 329–338, 1982.

Das, S., and B. V. Kostrov, Inversion of seismic slip rate history and distribution with stabilizing constraints: Application to the 1986 Andreanof Islands earthquake, *J. Geophys. Res.*, *95*, 6899–6913, 1990.

Dziewonski, A. M., G. Ekström, and M. P. Salganik, Centroid-moment tensor solutions for April-June 1994, *Phys. Earth Planet. Inter*, *88*, 69–78, 1995.

Ebel, J. E., Source processes of the 1965 New Hebrides Islands earthquakes inferred from teleseismic waveforms, *Geophys. J. R. Astron. Soc.*, *63*, 381–403, 1980.

Ebel, J. E., and A. L. Kafka, A Monte Carlo approach to seismic hazard analysis, *Bull Seismol. Soc. Am.*, *89*, 854–866, 1999.

Ellsworth, W. L., M. V. Mathews, R. M. Nadeau, S. P. Nishenko, P. A. Reasenberg, and R. W. Simpson, A physically-based earthquake recurrence model for estimation of long-term earthquake probabilities, paper presented at the Workshop on Earthquake Recurrence: State of the Art and Directions for the Future, Ist. Naz. de Geofis., Rome, Feb. 22–25 1999.

Filonov, A. E., Tsunami waves on the shelf near the west coast of Mexico (October 9, 1995), *Izv. Atmos. Oceanic Phys.*, *35*, 370–380, 1999.

Frankel, A., High-frequency spectral falloff of earthquakes, fractal dimension of complex rupture, *b* value, and the scaling of strength on faults, *J. Geophys. Res.*, *96*, 6291–6302, 1991.

Freund, L. B., and D. M. Barnett, A two-dimensional analysis of surface deformation due to dip-slip faulting, *Bull. Seismol. Soc. Am.*, *66*, 667–675, 1976.

Fujima, K., R. Dozono, and T. Shigemura, Generation and propagation of tsunami accompanying edge waves on a uniform sloping shelf, *Coastal Eng. J.*, *42*, 211–236, 2000.

Fukao, Y., and M. Furumoto, Hierarchy in earthquake size distribution, *Phys. Earth Planet. Inter.*, *37*, 149–168, 1985.

Fuller, J. D., and L. A. Mysak, Edge waves in the presence of an irregular coastline, *J. Phys. Oceanogr.*, *7*, 846–855, 1977.

Geist, E. L., Local tsunamis and earthquake source parameters, in *Tsunamigenic Earthquakes and Their Consequences*, *Adv. Geophys.*, vol. 39, edited by R. Dmowska and B. Saltzman, pp. 117–209, Academic, San Diego, Calif., 1998.

Geist, E. L., and R. Dmowska, Local tsunamis and distributed slip at the source, *Pure Appl. Geophys.*, *154*, 485–512, 1999.

Geist, E. L., and S. L. Bilek, Effect of depth-dependent shear modulus on tsunami generation along subduction zones, *Geophys. Res. Lett.*, *28*, 1315–1318, 2001.

González, F. I., K. Satake, F. Boss, and H. O. Mofjeld, Edge wave and non-trapped modes of the 25 April 1992 Cape Mendocino tsunami, *Pure Appl. Geophys.*, *144*, 409–426, 1995.

Hanks, T. C., *b* values and $\omega^{-\gamma}$ seismic source models: Implications for tectonic stress variations along active crustal fault zones and the estimation of high-frequency strong ground motion, *J. Geophys. Res.*, *84*, 2235–2242, 1979.

Hartzell, S. H., and T. H. Heaton, Teleseismic time functions for large, shallow, subduction zone earthquakes, *Bull. Seismol. Soc. Am.*, *75*, 965–1004, 1985.

Hartzell, S., and C. Langer, Importance of model parameterization in finite fault inversions: Application to the 1974 M_W 8.0 Peru earthquake, *J. Geophys. Res.*, *98*, 22,123–22,134, 1993.

Hartzell, S., P. C. Liu, and C. Mendoza, The 1994 Northridge, California, earthquake: Investigation of rupture velocity, risetime, and high-frequency radiation, *J. Geophys. Res.*, *101*, 20,091–20,108, 1996.

Hartzell, S., S. Harmsen, A. Frankel, and S. Larsen, Calculation of broadband time histories of ground motion: Comparison of methods and validation using strong-ground motion from the 1994 Northridge earthquake, *Bull. Seismol. Soc. Am.*, *89*, 1484–1504, 1999.

Herrero, A., and P. Bernard, A kinematic self-similar rupture process for earthquakes, *Bull. Seismol. Soc. Am.*, *84*, 1216–1228, 1994.

Huang, J., and D. L. Turcotte, Fractal distributions of stress and strength and variations of *b*-value, *Earth Planet. Sci. Lett.*, *91*, 223–230, 1988.

Ihmlé, P. F., Monte Carlo slip inversion in the frequency domain: Application to the 1992 Nicaragua slow earthquake, *Geophys. Res. Lett.*, *23*, 913–916, 1996.

Ihmlé, P. F., and J. C. Ruegg, Source tomography by simulated annealing using broad-band surface waves and geodetic data: Application to the M_W = 8.1 Chile 1995 event, *Geophys. J. Int.*, *131*, 146–158, 1997.

Ihmlé, P. F., J. M. Gomez, P. Heinrich, and S. Guibourg, The 1996 Peru tsunamigenic earthquake: Broadband source process, *Geophys. Res. Lett.*, *25*, 2691–2694, 1998.

Iida, K., Magnitude, energy, and generation mechanisms of tsunamis and a catalogue of earthquakes associated with tsunamis, in *Proceedings, Tsunami Meetings Associated with the Tenth Pacific Science Congress*, pp. 7–18, Int. Union of Geod. and Geophys., Paris, 1963.

Iida, K., D. C. Cox, and G. Pararas-Carayannis, Preliminary catalog of tsunamis occurring in the Pacific Ocean, *Data Rep. 5, HIG-67-10*, 274 pp., Univ. of Hawaii, Honolulu, 1967.

Imamura, F., E. Gica, T. Takahashi, and N. Shuto, Numerical simulation of the 1992 Flores tsunami: Interpretation of tsunami phenomena in northeastern Flores Island and damage at Babi Island, *Pure Appl. Geophys.*, *144*, 555–568, 1995.

Ishii, H., and K. Abe, Propagation of tsunami on a linear slope between two flat regions, part I, Edge wave, *J. Phys. Earth*, *28*, 531–541, 1980.

Johnson, J. M., and K. Satake, Source parameters of the 1957 Aleutian earthquake from tsunami waveforms, *Geophys. Res. Lett.*, *20*, 1487–1490, 1993.

Johnson, J. M., and K. Satake, Rupture extent of the 1938 Alaskan earthquake as inferred from tsunami waveforms, *Geophys. Res. Lett.*, *21*, 733–736, 1994.

Johnson, J. M., and K. Satake, The 1965 Rat Islands earthquake: A critical comparison of seismic and tsunami wave inversions, *Bull. Seismol. Soc. Am.*, *86*, 1229–1237, 1996.

Johnson, J. M., and K. Satake, Estimation of seismic moment and slip distribution of the April 1, 1946, Aleutian tsunami earthquake, *J. Geophys. Res.*, *102*, 11,765–11,774, 1997.

Johnson, J. M., K. Satake, S. R. Holdahl, and J. Sauber, The 1964 Prince William Sound earthquake: Joint inversion of tsunami and geodetic data, *J. Geophys. Res.*, *101*, 523–532, 1996.

Kajiura, K., The leading wave of a tsunami, *Bull. Earthquake Res. Inst. Univ. Tokyo*, *41*, 535–571, 1963.

Kanamori, H., Focal mechanism of the Tokachi-Oki earthquake of May 16, 1968: Contortion of the lithosphere at a junction of two trenches, *Tectonophysics*, *12*, 1–13, 1971.

Kanamori, H., Mechanism of tsunami earthquakes, *Phys. Earth Planet. Inter.*, *6*, 346–359, 1972.

Kanamori, H., and J. W. Given, Use of long-period surface waves for fast determination of earthquake source parameters, *Phys. Earth Planet. Inter.*, *27*, 8–31, 1981.

Kanamori, H., and M. Kikuchi, The 1992 Nicaragua earthquake: A slow tsunami earthquake associated with subducted sediments, *Nature*, *361*, 714–716, 1993.

Koyama, J., General description of the complex faulting process and some empirical relations in seismology, *J. Phys. Earth.*, *42*, 103–148, 1994.

Lahr, J. C., C. D. Stephens, H. S. Hasegawa, and J. Boatwright, Alaskan seismic gap only partially filled by 28 February 1979 earthquake, *Science*, *207*, 1351–1353, 1980.

Lander, J. F., Tsunamis affecting Alaska 1737–1996, *NGDC Key Geophys. Res. Doc.31*, 195 pp., Natl. Geophys. Data Cent., Natl. Oceanic and Atmos. Admin., Boulder, Colo., 1996.

Lay, T., and H. Kanamori, Earthquake doublets in the Solomon Islands, *Phys. Earth Planet. Inter.*, *2*, 283–304, 1980.

Lay, T., H. Kanamori, and L. Ruff, The asperity model and the nature of large subduction zone earthquakes, *Earthquake Predict. Res.*, *1*, 3–71, 1982.

Linde, A. T., and P. G. Silver, Elevation changes and the Great 1960 Chilean earthquake: Support for aseismic slip, *Geophys. Res. Lett.*, *16*, 1305–1308, 1989.

Lockridge, P. A., Tsunamis in Peru-Chile, *Publ. SE-39*, 97 pp., World Data Cent. A for Solid Earth Geophys., Natl. Geophys. Data Cent., Natl. Oceanic and Atmos. Admin., Boulder, Colo., 1985.

Lockridge, P. A., and R. H. Smith, *Tsunamis in the Pacific Basin, 1900–1983*, Natl. Geophys. Data Cent., Natl. Oceanic and Atmos. Admin., Boulder, Colo., 1984.

Mai, P. M., and G. C. Beroza, Source scaling properties from finite-fault-rupture models, *Bull. Seismol. Soc. Am.*, *90*, 604–615, 2000.

Malgrange, M., A. Deschamps, and R. Madariaga, Thrust and extensional faulting under the Chilean coast; 1965, 1971 Aconcagua earthquakes, *Geophys. L. R. Astron. Soc.*, *66*, 313–332, 1981.

Mandelbrot, B. B., *The Fractal Geometry of Nature*, 460 pp., W. H. Freeman, New York, 1977.

Mendoza, C., Coseismic slip of two large Mexican earthquakes from teleseismic body waveforms: Implications for asperity interaction in the Michoacan plate boundary segment, *J. Geophys. Res.*, *98*, 8197–8210, 1993.

Mendoza, C., Finite-fault analysis of the 1979 March 14 Petatlan, Mexico, earthquake using teleseismic *P* waveforms, *Geophys. J. Int.*, *121*, 675–683, 1995.

Mendoza, C., and E. Fukuyama, The July 12, 1993, Hokkaido-Nansei-Oki, Japan, earthquake: Coseismic slip pattern from strong-motion and teleseismic recordings, *J. Geophys. Res.*, *101*, 791–801, 1996.

Mendoza, C., and S. Hartzell, Slip distribution of the 19 September 1985 Michoacan, Mexico, earthquake; near-source and teleseismic constraints, *Bull. Seismol. Soc. Am.*, *79*, 655–669, 1989.

Mendoza, C., and S. Hartzell, Fault-slip distribution of the 1995 Colima-Jalisco, Mexico, earthquake, *Bull. Seismol. Soc. Am.*, *89*, 1338–1344, 1999.

Mendoza, C., S. Hartzell, and T. Monfret, Wide-band analysis of the 3 March 1985 central Chile earthquake, *Bull. Seismol. Soc. Am.*, *84*, 269–283, 1994.

Myers, E. P., and A. M. Baptista, Finite element modeling of the July 12, 1993 Hokkaido Nansei-Oki Tsunami, *Pure Appl. Geophys.*, *144*, 769–802, 1995.

National Geophysical Data Center, World-wide tsunamis, 2000 B.C.–1996, Boulder, Colo., 1996.

Okada, Y., Surface deformation due to shear and tensile faults in a half-space, *Bull. Seismol. Soc. Am.*, *75*, 1135–1154, 1985.

Okal, E. A., Mode-wave equivalence and other asymptotic problems in tsunami theory, *Phys. Earth Planet. Inter.*, *30*, 1–11, 1982.

Ortiz, M., V. Kostoglodov, S. K. Singh, and J. Pacheco, New constraints on the uplift of October 9, 1995 Jalisco-Colima earthquake (M_w 8) based on the analysis of tsunami records at Manzanillo and Navidad, *Geofis. Int.*, *39*, 349–357, 2000.

Pacheco, J. F., L. R. Sykes, and C. H. Scholz, Nature of seismic coupling along simple plate boundaries of the subduction type, *J. Geophys., Res.*, *98*, 14,133–14,159, 1993.

Peitgen, H. O., H. Jürgens, and D. Saupe, *Chaos and Fractals: New Frontiers of Science*, 984 pp., Springer-Verlag, New York, 1992.

Pelayo, A. M., and D. A. Wiens, Tsunami earthquakes: slow thrust-faulting events in the accretionary wedge, *J. Geophys. Res.*, *97*, 15,321–15,337, 1992.

Pelinovsky, E. N., and R. K. Mazova, Exact analytical solutions of nonlinear problems of tsunami wave run-up on slopes with different profiles, *Nat. Hazards*, *6*, 227–249, 1992.

Polet, J., and H. Kanamori, Shallow subduction zone earthquakes and their tsunamigenic potential, *Geophys. J. Int.*, *142*, 684–702, 2000.

Rabinovich, A. B., Spectral analysis of tsunami waves: Separation of source and topography effects, *J. Geophys. Res.*, *102*, 12,663–12,676, 1997.

Ramirez, J., and H. Titichoca, The minor destructive tsunami occurring near Antofagasta, northern Chile, July 20, 1995, *Sci. Tsunami Hazards*, *15*, 3–21, 1997.

Reid, R. O., and B. R. Bodine, Numerical model for storm surges in Galveston Bay, *J. Waterway Harbor Div. Am. Soc. Civ. Eng.*, *94*, 33–57, 1968.

Rudnicki, J. W., and M. Wu, Mechanics of dip-slip faulting in an elastic half-space, *J. Geophys. Res.*, *100*, 22,173–22,186, 1995.

Rundle, J. B., and H. Kanamori, Application of an inhomogeneous stress (patch) model to complex subduction zone earthquakes: A discrete interaction matrix approach, *J. Geophys. Res.*, *92*, 2606–2616, 1987.

Rydelek, P. A., and I. S. Sacks, Earthquake slip rise time and rupture propagation: Numerical results of the quantum earthquake model, *Bull. Seismol. Soc. Am.*, *86*, 567–574, 1996.

Sanchez, A. J., and S. F. Farreras, Catalog of tsunamis on the western coast of Mexico, *Publ. SE-50*, 79 pp., World Data Cent. A for Solid Earth Geophys., Natl. Geophys. Data Cent., Boulder, Colo., 1993.

Satake, K., Depth distribution of coseismic slip along the Nankai trough, Japan, from joint inversion of geodetic and tsunami data, *J. Geophys. Res.*, *98*, 4553–4565, 1993.

Satake, K., Mechanism of the 1992 Nicaragua tsunami earthquake, *Geophys. Res. Lett.*, *21*, 2519–2522, 1994.

Satake, K., Linear and nonlinear computations of the 1992 Nicaragua earthquake tsunami, *Pure Appl. Geophys.*, *144*, 455–470, 1995.

Satake, K., and H. Kanamori, Use of tsunami waveforms for earthquake source study, *Nat. Hazards*, *4*, 193–208, 1991.

Satake, K., and Y. Tanioka, Tsunami generation of the 1993 Hokkaido Nansei-Oki earthquake, *Pure Appl. Geophys.*, *144*, 803–821, 1995.

Satake, K., and Y. Tanioka, Sources of tsunami and tsunamigenic earthquakes in subduction zones, *Pure Appl. Geophys.*, *154*, 467–483, 1999.

Savage, J. C., Displacement field for an edge dislocation in a layered half-space, *J. Geophys. Res.*, *103*, 2439–2446, 1998.

Seno, T., K. Shimazaki, P. Somerville, K. Sudo, and T. Eguchi, Rupture process of the Miyagi-Oki, Japan, earthquake of June 12, 1978, *Phys. Earth Planet. Inter*, *23*, 39–61, 1980.

Sezawa, K., and K. Kanai, On shallow water waves transmitted in the direction parallel to a sea coast, with special reference to Love-waves in heterogeneous media, *Bull. Earthquake Res. Inst. Univ. Tokyo*, *17*, 685–694, 1939.

Shimazaki, K., Nemuro-Oki earthquake of June 17, 1973: A lithospheric rebound at the upper half of interface, *Phys. Earth Planet. Inter.*, *39*, 314–327, 1974.

Shimazaki, K., Small and large earthquakes: The effects of the thickness of seismogenic layer and the free surface, in *Earthquake Source Mechanics*, Geophys. Monogr. Ser., vol. 37, edited by S. Das, J. Boatwright, and C. Scholz, pp. 209–216, AGU, Washington, D. C., 1986.

Shono, K., T. Mikumo, and Y. Ishikawa, Focal mechanisms of earthquakes in Hyuga-nada and Ryukyu arc and their tectonic implications, *Program Abstr. Seismol. Soc. Jpn.*, *2*, 71, 1976.

Shuto, N., Numerical simulation of tsunamis—Its present and near future, *Nat. Hazards*, *4*, 171–191, 1991.

Soloviev, S. L., Recurrence of tsunamis in the Pacific, in *Tsunamis in the Pacific Ocean*, edited by W. M. Adams, pp. 149–163, East-West Cent., Honolulu, Hawaii, 1970.

Soloviev, S. L., and C. N. Go, *A Catalogue of Tsunamis on the Western Shore of the Pacific Ocean*, 310 pp., Russ. Acad. of Sci., Moscow, 1974. (*Can. Transl. Fish. Aquat. Sci.5077*, 1984.)

Somerville, P., K. Irikura, R. Graves, S. Sawada, D. Wald, N. Abrahamson, Y. Iwasaki, T. Kagawa, N. Smith, and A. Kowada, Characterizing crustal earthquake slip models for the prediction of strong ground motion, *Seismol. Res. Lett.*, *70*, 59–80, 1999.

Stewart, G. S., and S. N. Cohn, The 1976 August 16, Mindanao, Philippine earthquake (M_s = 7.8): Evidence for a subduction zone south of Mindanao, *Geophys. J. R. Astron. Soc.*, *57*, 51–65, 1979.

Stewart, G. S., E. P. Chael, and K. C. McNally, The November 29, 1978, Oaxaca, Mexico, earthquake; a large simple event, *J. Geophys. Res.*, *86*, 5053–5060, 1981.

Suárez, G., and O. Sánchez, Shallow depth of seismogenic coupling in southern Mexico: Implications for the maximum size of earthquakes in subduction zones, *Phys. Earth Planet. Inter.*, *93*, 53–61, 1996.

Tadepalli, S., and C. E. Synolakis, The run-up of *N*-waves on sloping beaches, *Proc. R. Soc. London, Ser. A*, *445*, 99–112, 1994.

Tadepalli, S., and C. E. Synolakis, Model for the leading waves of tsunamis, *Phys. Rev. Lett.*, *77*, 2141–2144, 1996.

Tanioka, Y., and K. Satake, Fault parameters of the 1896 Sanriku tsunami earthquake estimated from tsunami numerical modeling, *Geophys. Res. Lett.*, *23*, 1549–1552, 1996.

Tanioka, Y., L. Ruff, and K. Satake, The Sanriku-oki, Japan, earthquake of December 28, 1994 (M_W 7.7): Rupture of a different asperity from a previous earthquake, *Geophys. Res. Lett.*, *23*, 1465–1468, 1996.

Thatcher, W., Order and diversity in the modes of circum-Pacific earthquake recurrence, *J. Geophys. Res.*, *95*, 2609–2623, 1990.

Tichelaar, B. W., and L. J. Ruff, Depth of seismic coupling along subduction zones, *J. Geophys. Res.*, *98*, 2017–2037, 1993.

Titov, V. V., and C. E. Synolakis, Extreme inundation flows during the Hokkaido-Nansei-Oki tsunami, *Geophys. Res. Lett.*, *24*, 1315–1318, 1997.

Togashi, H., Shoreline wave height and land run-up height of tsunamis on uniformly sloping beaches, in *Tsunamis: Their Science and Engineering*, edited by J. Iida and T. Iwasaki, pp. 495–509, Terra Sci., Tokyo, 1983.

Tsai, C. P., Slip, stress drop and ground motion of earthquakes: A view from the perspective of fractional brownian motion, *Pure Appl. Geophys*, *149*, 689–706, 1997.

Tsuji, Y., F. Imamura, H. Matsutomi, C. E. Synolakis, P. T. Nanang, S. Jumadi, S. Harada, S. S. Han, K. Arai, and B. Cook, Field survey of the east Java earthquake and tsunami of June 3, 1994, *Pure Appl. Geophys.*, *144*, 839–854, 1995.

Turcotte, D. L., *Fractals and Chaos in Geology and Geophysics*, 221 pp., Cambridge Univ. Press, New York, 1992.

Wald, D. J., and P. G. Somerville, Variable-slip rupture model of the great 1923 Kanto, Japan earthquake: Geodetic and body-waveform analysis, *Bull. Seismol. Soc. Am.*, *85*, 159–177, 1995.

Ward, S. N., Relationships of tsunami generation and an earthquake source, *J. Phys. Earth*, *28*, 441–474, 1980.

Ward, S. N., Landslide tsunami, *J. Geophys. Res.*, *106*, 11,201–11,215, 2001a.

Ward, S. N., Tsunamis, in *Encyclopedia of Physical Science and Technology*, vol. 17, edited by R. A. Meyers, Academic, San Diego, Calif., 2001b.

Ward, S. N., and E. Asphaug, Asteroid impact tsunami: A probabilistic hazard assessment, *Icarus*, *145*, 64–78, 2000.

Yoshioka, N., and K. Abe, Focal mechanism of the Iwate-Oki earthquake of June 12, 1968, *J. Phys. Earth*, *24*, 251–262, 1976.

Yoshioka, S., M. Hashimoto, and K. Hirahara, Displacement fields due to the 1946 Nankaido earthquake in a laterally inhomogeneous structure with the subducting Philippine Sea plate—A three-dimensional finite element approach, *Tectonophysics*, *159*, 121–136, 1989.

E. L. Geist, U.S. Geological Survey, 345 Middlefield Road, MS 999, Menlo Park, CA 94025, USA. (egeist@usgs.gov)

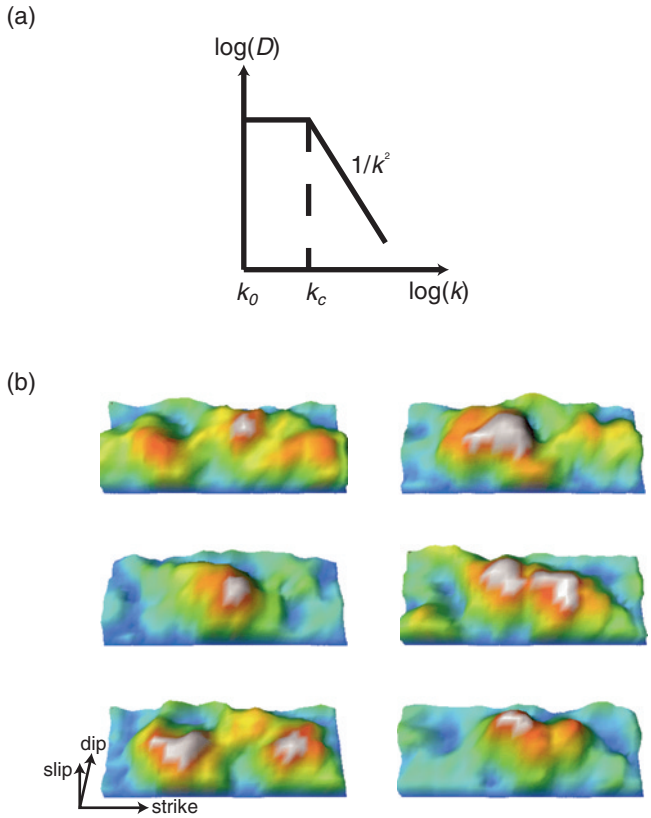

Figure 3. (a) Model radial wave number (k) spectrum for the synthetic slip distributions used in this study [*Herrero and Bernard*, 1994]. The k^{-2} falloff at high wave numbers is consistent with ω^{-2} model for the seismic source spectrum [*Aki*, 1967]. The parameter k_c is the corner wave number of the slip spectrum; k_0 is the fundamental wave number for the discrete spectrum. (b) Slip distributions produced by the stochastic model illustrating the diversity of slip distribution patterns. Light colors represent high amounts of slip.